arXiv:0803.2348v1 [gr-qc] 16 Mar 2008

Binary Black Hole Coalescence in Semi-Analytic Puncture Evolution

Achamveedu Gopakumar and Gerhard Schäfer
Theoretisch-Physikalisches Institut, Friedrich-Schiller-Universität Jena, Max-Wien-Platz 1, 07743 Jena, Germany

(Dated: March 16, 2008)

Binary black-hole coalescence is treated semi-analytically by a novel approach. Our prescription employs the conservative Skeleton Hamiltonian that describes orbiting Brill-Lindquist wormholes (termed punctures in Numerical Relativity) within a waveless truncation to the Einstein field equations [G. Faye, P. Jaranowski and G. Schäfer, Phys. Rev. D **69**, 124029 (2004)]. We incorporate, in a transparent Hamiltonian way and in Burke-Thorne gauge structure, the effects of gravitational radiation reaction into the above Skeleton dynamics with the help of 3.5PN accurate angular momentum flux for compact binaries in quasi-circular orbits to obtain a Semi-Analytic Puncture Evolution to model merging black-hole binaries. With the help of the TaylorT4 approximant at 3.5PN order, we perform a *first-order* comparison between gravitational wave phase evolutions in Numerical Relativity and our approach for equal-mass binary black holes. This comparison reveals that a modified Skeletonian reactive dynamics that employs flexible parameters will be required to prevent the dephasing between our scheme and Numerical Relativity, similar to what is pursued in the Effective One Body approach. A rough estimate for the gravitational waveform associated with the binary black-hole coalescence in our approach is also provided.

PACS numbers: 04.30.Db, 04.25.Nx

I. INTRODUCTION

Binary black hole mergers are the most plausible sources of gravitational radiation for the currently operational and planned ground-based laser interferometric gravitational-wave (GW) detectors like GEO-LIGO and VIRGO. Further, coalescing binary black holes (BBH) are considered to be the workhorse sources to realize GW astronomy with the proposed space-based GW interferometer LISA. Recent advances in Numerical Relativity, achieved by several independent groups, should enable its practitioners to create accurate and 'exact' numerical relativity based GW search templates for the late stages of binary black hole coalescence [1]. However, it is also desirable to develop semi-analytic prescriptions, based on well defined assumptions, capable of describing the most relativistic part of the binary black hole coalescence, namely the last few cycles of the inspiral, plunge and the subsequent merger. The two main reasons to develop such descriptions are as follows. It is reasonable to imagine that semi-analytic approaches, based on certain assumptions, should be able to probe the purely numerical approaches in order to extract the 'physics' behind binary black hole coalescence. The second reason is related to the GW data analysis requirement of creating huge banks of accurate GW templates to cover, rather densely, the binary black hole parameter space.

In the literature and to best of our knowledge, there exists only two approaches that can semi-analytically model the late stages of non-spinning compact binary coalescence. Historically, the first prescription is the so-called hybrid approach, developed by Will and his collaborators, which re-sums exactly the 'Schwarzschild terms' in the post-Newtonian(PN) accurate equations of motion for compact binaries and treats the symmetric mass ratio terms as additional corrections [2]. The second and widely employed approach is the so-called Effective One-Body (EOB) scheme, developed by Damour and collaborators [3, 4]. The EOB scheme requires available PN accurate results for the conservative orbital dynamics and GW luminosity associated with comparable mass compact binaries moving along quasi-circular orbits extractable from Refs. [5]. In the EOB approach, one packages these PN accurate results in a certain re-summed form with the hope of extending the validity of PN accurate results to strong-field (and fast-motion) regimes. The EOB package allows PN accurate dynamics of a comparable mass compact binary, having masses m_1 and m_2, to be mapped onto an essentially geodesic dynamics of a test-particle of mass $\mu = m_1\, m_2/(m_1+m_2)$ moving in an $\eta = m_1\, m_2/(m_1+m_2)^2$ deformed Schwarzschild geometry. Further, reactive dynamics is included with the help of certain Padé re-summed radiation reaction force. It is important to note that in the hybrid and EOB approaches, describing late stages of binary black hole coalescence, essentially contain a single black hole and some undesirable features of these schemes were pointed out in Refs. [6] and [7].

In this paper, we present a prescription that can semi-analytically model the late stages of coalescing non-spinning binary black holes (BBH). Our approach employs the 'Skeleton' solution to the Einstein field equations, detailed in Ref. [8], to describe the BBH conservative dynamics. We augment the above mentioned BBH conservative dynamics by incorporating radiation reaction effects in a fully Hamiltonian way with the help of the 3.5PN accurate GW luminosity, available in Refs. [5]. This is how, in a nutshell, we provide a semi-analytical description for the late stages of BBH coalescence. The fact that the Skeleton Hamiltonian is constructed in the Arnowitt-Deser-Misner (ADM) 3+1 approach to General Relativity [9] makes our scheme very close to the BBH dynamics, analyzed by several Numerical Relativity groups. The Skeleton Hamiltonian contains, in its static part, the potential of the well-known Brill-Lindquist BBH initial value configuration [10, 11]. Further, it allows black holes to orbit each other along conservative orbital configurations. We emphasize that the above mentioned conservative orbital evolution obey exactly only a truncated version of Einstein's field equations [8]. In the Skeleton approach for black holes in circular orbits, Ref. [8] also demonstrated an intriguing property; the ADM mass (identified through the 3-metric) [9] coincides with the Komar mass (identified through the pure time component of the 4-metric)[12]. We note that the equality of ADM and Komar masses is a general property of stationary solutions to the Einstein field equations for isolated systems. This is, in our view, an appealing feature of the Skeleton scheme.

In Numerical Relativity simulations that employ punctures to model black holes, it is customary to use Brill-Lindquist configurations as initial data [13]. Therefore, the unique construction of the Skeleton Hamiltonian for BBH, based on certain well defined assumptions, and its present extension should allow us to probe the various aspects of Numerical Relativity based BBH simulations involving punctures. This prompted us to name our approach as Semi-Analytic Puncture Evolution (SAPE). However, it should be noted that the recent Numerical Relativity simulations involving black holes do not impose conformal flat condition in their evolutions, required by our SAPE.

The organization of this paper is as follows. In the next section, we briefly summarize the Skeleton approximation and the conservative binary black hole dynamics it defines, detailed in Ref. [8]. Section II also includes a fully consistent Hamiltonian way of incorporating the effects of radiation reaction on to the conservative Skeleton dynamics. The resulting binary black hole dynamics and its implications are explored in Section III. An estimate for the complete gravitational wave polarizations associated with the binary black hole coalescence in reactive Skeleton dynamics, in the 'restricted waveform' approach, is presented in Section IV. Our conclusions and future directions are available in Section V.

II. BINARY PUNCTURE DYNAMICS IN SKELETON APPROXIMATION

In this section, we briefly summarize the construction of the conservative binary black hole Skeleton Hamiltonian, detailed in Ref. [8]. Afterwards, we explain our prescription for including the effects of GW radiation reaction into the Skeletonian conservative dynamics.

A. Conservative Skeletonian Binary Black Hole Dynamics

In the ADM formulation of General Relativity, the spacetime line element in the $(3+1)$ decomposed form is given by

$$ds^2 = -\alpha^2 c^2 dt^2 + \gamma_{ij}(dx^i + \beta^i c dt)(dx^j + \beta^j c dt) \quad (\, i,j = 1,2,3 \,) \, , \tag{1}$$

where α is the lapse function, β^i the shift vector, γ_{ij} the induced metric on a three-dimensional spatial slice $\Sigma(t)$, parametrized by the time coordinate t, and c is the velocity of light. The canonical conjugate to the 3-metric γ_{ij} is given by $\pi^{ij} c^3/16\pi G$, where G is the Newtonian gravitational constant and it is a tensor density of weight $+1$. Further, γ_{ij} and π^{ij} satisfy the Hamiltonian and momentum constraints [9]. On any three-dimensional spatial slice $\Sigma(t)$, the above four constraints may be written as

$$\gamma^{1/2}\mathrm{R} - \frac{1}{\gamma^{1/2}}\left(\pi^i_j \pi^j_i - \frac{1}{2}\pi^2\right) = \frac{16\pi G}{c^3}\sum_a \left(m_a^2 c^2 + \gamma^{ij} p_{ai} p_{aj}\right)^{1/2} \delta_a \, , \tag{2a}$$

$$-2\partial_j \pi^j_i + \pi^{kl}\partial_i \gamma_{kl} = \frac{16\pi G}{c^3}\sum_a p_{ai}\delta_a \, , \tag{2b}$$

where R, γ, γ^{ij} stand respectively for the curvature scalar, the determinant, the inverse metric associated with the 3-metric γ_{ij}. The linear momentum of point-mass a (a=1,2) is denoted by p_{ai} and its bare mass by m_a. The partial derivative with respect to the hypersurface coordinates is denoted by $\partial_i = \partial/\partial x^i$. The Dirac delta function $\delta_a = \delta(x^i - x^i_a(t))$ is defined by $\delta(x^i - x^i_a(t)) = 0$ if $x^i \neq x^i_a(t)$ and $\int d^3x \; \delta(x^i - x^i_a(t)) = 1$, where $x^i_a(t)$ is the space coordinate of point-mass a at time t.

The ADM coordinate conditions that generalize the isotropic Schwarzschild metric read

$$\gamma_{ij} = \left(1 + \frac{1}{8}\phi\right)^4 \delta_{ij} + h^{\mathrm{TT}}_{ij} \, , \tag{3a}$$

$$\pi^{ii} = 0 \, , \tag{3b}$$

where ϕ is a function vanishing at spatial infinity. The tranverse-traceless (TT) part of the metric γ_{ij} with respect to the Euclidean 3-metric δ_{ij} is denoted by h^{TT}_{ij} and the Einstein summation convention is also employed in the above equation, $\pi^{ii} = 0$. Taking into account the above gauge condition for π^{ij}, the following decomposition can be achieved:

$$\pi^{ij} = \tilde{\pi}^{ij} + \pi^{ij}_{\mathrm{TT}} \, , \tag{4}$$

where $\tilde{\pi}^{ij}$ denotes the longitudinal part of π^{ij} which may be expressed as

$$\tilde{\pi}^{ij} = \partial_i \pi^j + \partial_j \pi^i - \frac{2}{3}\delta_{ij}\partial_k \pi^k \, , \tag{5}$$

where π^i is a vector in the flat 3-space. Further, the TT part of π^{ij}, or rather $\pi^{ij}_{\rm TT}c^3/16\pi G$, provides the canonical conjugate to $h^{\rm TT}_{ij}$.

The Hamilton functional for non-spinning binary black hole system is given by

$$\begin{aligned} H\Big[x^i_a, p_{ai}, h^{\rm TT}_{ij}, \pi^{ij}_{\rm TT}\Big] = -\frac{c^4}{16\pi G}\int d^3x\ \Delta\phi\Big[x^i_a, p_{ai}, \\ h^{\rm TT}_{ij}, \pi^{ij}_{\rm TT}\Big]\,, \end{aligned} \tag{6}$$

where Δ is the Laplacian in the 3-dimensional flat space. While dealing with the dynamics of binary black-hole systems, it is highly advantageous to introduce a Routh functional of the form,

$$R\left[x^i_a, p_{ai}, h^{\rm TT}_{ij}, \partial_t h^{\rm TT}_{ij}\right] = H - \frac{c^3}{16\pi G}\int d^3x\ \pi^{ij}_{\rm TT}\partial_t h^{\rm TT}_{ij}\,. \tag{7}$$

This functional is a Hamiltonian for the particle (point-mass) degrees of freedom, and a Lagrangian for the independent gravitational field degrees of freedom. The truncation implemented in Ref. [8], *i.e.* to put $h^{\rm TT}_{ij} \equiv 0$, is called the conformal flat condition and it results in $H = R(x^i_a, p_{ai})$.

It is possible to show that the introduced source model, namely δ_a terms in Eqs. (2), can produce certain binary black-hole spacetime. Indeed, it was demonstrated in Refs. [11] that one obtains the Brill-Lindquist initial value solution for uncharged black holes at rest, available in Ref. [10]. Therefore, let us first summarize Refs. [11]. In Refs. [11], one imposes $h^{\rm TT}_{ij} = 0$ and $p_{ai} = 0$ (and this leads to $\pi^{ij} = 0$). Under these restrictions, the Hamiltonian constraint becomes

$$-\left(1 + \frac{1}{8}\ \phi\right)\Delta\phi = \frac{16\pi G}{c^2}\sum_a m_a\delta_a. \tag{8}$$

The exact (and unique) solution to the above equation, detailed in Ref. [11] and obtained with the help of dimensional regularization, reads

$$\phi = \frac{4G}{c^2}\sum_a\frac{\alpha_a}{r_a}\,, \quad \text{where} \tag{9a}$$

$$\begin{aligned} \alpha_a = \frac{m_a - m_b}{2} + \frac{c^2 r_{ab}}{G}\Bigg\{\Bigg[1 + \frac{m_a + m_b}{c^2 r_{ab}/G} + \\ \left(\frac{m_a - m_b}{2c^2 r_{ab}/G}\right)^2\Bigg]^{1/2} - 1\Bigg\} \end{aligned} \tag{9b}$$

and r_a denotes the Euclidean distance between x^i and x^i_a and r_{ab} the Euclidean distance between x^i_a and x^i_b.

The Brill-Lindquist potential function, computed in Refs. [11], reads

$$H_{\rm BL} = (\alpha_1 + \alpha_2)\ c^2 = (m_1 + m_2)\ c^2 - G\ \frac{\alpha_1\alpha_2}{r_{12}}\,, \tag{10}$$

and as expected it describes the total (initial) energy between two uncharged Brill-Lindquist black holes.

The Skeleton approach to General Relativity for dealing with BBH space-times, detailed Ref. [8], requires both the conformal flat condition/truncation for the spatial 3-metric and hereof together with Eq. (3b) the maximal slicing condition. These prescriptions, valid for all times, are given by

$$\gamma_{ij} = (1 + \frac{1}{8}\phi)^4\delta_{ij}\,, \tag{11a}$$

$$\pi^{ij}\gamma_{ij} = 2\sqrt{\gamma}\gamma^{ij}K_{ij} = 0\,. \tag{11b}$$

In above equations, K_{ij} is the extrinsic curvature of $\Sigma(t)$ and is related to π^{ij} by $\pi^{ij} = -\gamma^{1/2}(\gamma^{il}\gamma^{jm} - \gamma^{ij}\gamma^{lm})K_{lm}$.

Under the above conditions, the momentum constraint equations for the Einstein theory become

$$\pi^j_{i,\,j} = -\frac{8\pi G}{c^3}\sum_a p_{ai}\delta_a\,. \tag{12}$$

The solution of this equation is constructed under the condition that π^j_i is of purely longitudinal form

$$\pi^j_i = \partial_i V_j + \partial_j V_i - \frac{2}{3}\delta_{ij}\partial_l V_l\,, \tag{13}$$

where V_i is a vector in the flat 3-space. The difference to the way $\tilde\pi^{ij}$ is defined, via Eq. (5), should be noted. In the Skeleton approach, π^i_j consists only of its longitudinal part and is defined in terms of V_i via Eq. (13). The Hamiltonian constraint in the Skeleton scheme becomes

$$\begin{aligned} \Delta\phi = -\frac{\pi^j_i\pi^i_j}{(1 + \frac{1}{8}\phi)^7} - \frac{16\pi G}{c^2}\sum_a\frac{m_a\delta_a}{(1 + \frac{1}{8}\phi)}\Bigg(1 + \\ \frac{p_a^2}{(1 + \frac{1}{8}\phi)^4 m_a^2 c^2}\Bigg)^{1/2}. \end{aligned} \tag{14}$$

Further, one implements a truncation to the numerator of the first term, namely $\pi^j_i\pi^i_j$, in the following manner

$$\begin{aligned} \pi^j_i\pi^i_j &\equiv -2V_j\partial_i\pi^i_j + \partial_i(2V_j\pi^i_j) \\ &\to -2V_j\partial_i\pi^i_j = \frac{16\pi G}{c^3}\sum_a p_{aj}V_j\delta_a\,. \end{aligned} \tag{15}$$

This is the other crucial truncation in addition to the conformal flat truncation required in the Skeleton approach. This truncation introduces errors of the same order as the conformal flat truncation. Therefore, in a post-Newtonian setting, the errors are of the 2PN order. With the aid of the ansatz

$$\phi = \frac{4G}{c^2}\sum_a\frac{\alpha_a}{r_a}\,, \tag{16}$$

which is inspired by the delta-function sources in Eq. (14), after the insertion of Eq. (15), the resulting energy constraint equation can be solved in the sense of dimensional regularization, detailed in Ref. [8]. This results in two coupled algebraic equations given by

$$\alpha_a = \frac{m_a}{1+\lambda \frac{\alpha_b}{r_{ab}}} \times \left[1 + \frac{p_a^2/(m_a^2 c^2)}{\left(1+\lambda \frac{\alpha_b}{r_{ab}}\right)^4} \right]^{\frac{1}{2}} + \frac{p_{ai} V_{ai}/c}{\left(1+\lambda \frac{\alpha_b}{r_{ab}}\right)^7}\,, \tag{17}$$

where $a = 1, 2$, $b \neq a$ and λ stands for $G/(2\,c^2)$. The α_a-parameters generalize the rest energies of interacting black holes at rest, given in Eq. (9b), to orbiting black holes.

With these inputs, the Skeleton Hamiltonian for BBH becomes

$$H_{\rm Sk} \equiv -\frac{c^4}{16\pi G} \int d^3x\, \Delta\phi = c^2 \sum_a \alpha_a\,. \tag{18}$$

The Hamilton equations of motion, as usual, read

$$\dot{\boldsymbol{x}}_a = \frac{\partial H}{\partial \boldsymbol{p}_a}\,, \qquad \dot{\boldsymbol{p}}_a = -\frac{\partial H}{\partial \boldsymbol{x}_a}\,. \tag{19}$$

For a binary system in the center-of-mass frame, we have

$$\boldsymbol{p_1} = -\boldsymbol{p_2} \equiv \boldsymbol{p}\,, \tag{20a}$$

$$\boldsymbol{r} \equiv \boldsymbol{x_1} - \boldsymbol{x_2}\,, \tag{20b}$$

$$r^2 = (\boldsymbol{x_1} - \boldsymbol{x_2}) \cdot (\boldsymbol{x_1} - \boldsymbol{x_2})\ . \tag{20c}$$

Further, we will employ the following convenient dimensionless quantities

$$\hat{t} = \frac{t\,c^3}{G\,m}\,,\ \hat{r} = \frac{r\,c^2}{G\,m}\,,\ \hat{\boldsymbol{p}} = \frac{\boldsymbol{p}}{\mu\,c}\,,\ \hat{\mathcal{H}}_{\rm Sk} = \frac{H_{\rm Sk}}{\mu\,c^2}\,, \tag{21a}$$

$$\hat{j} = \frac{J\,c}{G\,m\,\mu}\,,\ \hat{p}_r = \frac{p_r}{\mu\,c}\,,\ \hat{\boldsymbol{p}}^2 = \hat{p}_r^2 + \hat{j}^2/\hat{r}^2\,, \tag{21b}$$

where $\boldsymbol{J} = \boldsymbol{r} \times \boldsymbol{p}$ and $p_r = \boldsymbol{p} \cdot \boldsymbol{r}/r$.

For the purpose of present investigation and using Eqs. (5.1),(5.2) and (5.4) in Ref. [8], we write the Skeleton Hamiltonian $\hat{\mathcal{H}}_{\rm Sk}$ in the following way

$$\hat{\mathcal{H}}_{\rm Sk} = 2\,\hat{r}\left(\psi_1 + \psi_2 - 2\right), \text{where} \tag{22a}$$

$$\psi_1 = 1 + \frac{\chi_-}{4\,\hat{r}\,\psi_2}\left(1 + \frac{4\,\eta^2\left(\hat{p}_r^2 + \frac{\hat{j}^2}{\hat{r}^2}\right)}{\chi_-^2\,\psi_2^4}\right)^{1/2} - \frac{\left(8\,\hat{p}_r^2 + 7\,\frac{\hat{j}^2}{\hat{r}^2}\right)\eta^2}{8\,\hat{r}^2 {\psi_2}^7}\,, \tag{22b}$$

$$\psi_2 = 1 + \frac{\chi_+}{4\,\hat{r}\,\psi_1}\left(1 + \frac{4\,\eta^2\left(\hat{p}_r^2 + \frac{\hat{j}^2}{\hat{r}^2}\right)}{\chi_+^2\,\psi_1^4}\right)^{1/2} - \frac{\left(8\,\hat{p}_r^2 + 7\,\frac{\hat{j}^2}{\hat{r}^2}\right)\eta^2}{8\,\hat{r}^2 {\psi_1}^7}\,, \tag{22c}$$

and the symbols $\chi_{-/+}$ are defined to be $\chi_- = \left(1 - \sqrt{1-4\,\eta}\right)$ and $\chi_+ = \left(1 + \sqrt{1-4\,\eta}\right)$.

The conservative Skeleton Hamiltonian has the following features and properties. The Skeleton Hamiltonian is exact in the test-body limit, where it describes the motion of a test particle in the Schwarzschild spacetime. It is also identical to the 1PN accurate Hamiltonian describing the compact binary dynamics in General Relativity. Further, as explained earlier, when the point particles are at rest, the Brill-Lindquist initial value solution is reproduced. It is remarkable that the Skeleton Hamiltonian allows a post-Newtonian expansion in powers of $1/c^2$ to arbitrary orders. This is remarkable because of the observation that the 3PN approximate binary black hole Hamiltonian does not exist, if one only imposes the conformal flat condition without invoking Eq. (15) [8]. Therefore, the Skeleton Hamiltonian describes the evolution of punctures under both conformal flat conditions for the 3-metric and analyticity conditions for the Hamiltonian via PN expansions (and, of course, gravitational radiation reaction is not incorporated). The Skeleton dynamics is not isolated from the metric field rather it is embedded in the field [recall that the Skeleton Hamiltonian originates from γ_{ij}]. Furthermore, with the aid of similar truncations, it is also possible to calculate α and β^i [8] and, as expected, the demonstration of the equality of ADM and Komar masses for BBH in circular orbits in the Skelton approach requires explicit expressions for α and β^i. These arguments imply that in the Skelton scheme for BBH, a global spacetime picture exists.

B. Tackling the effects of radiation reaction

This subsection details how we incorporate radiation reaction effects into the above described conservative binary black hole dynamics. Our prescription is heavily influenced by the way the reactive 2.5PN Hamiltonian affects the conservative 2PN accurate compact binary dynamics. Therefore, let us first take a closer look at the way reactive contributions to $\mathcal{H}$ change Hamiltonian equations of motion in the post-Newtonian approximation with the help of 2.5PN accurate $\mathcal{H}$, available in Refs. [14, 15]. It is convenient (and usual) to split the fully 2.5PN accurate H as

$$H_{\rm 2.5PN} = H^{\rm c}_{\rm 2PN} + H^{\rm r}_{\rm 2.5PN}\,, \tag{23}$$

where $H^{\rm c}_{\rm 2PN}$ defines the 2PN accurate conservative orbital dynamics [15]. The explicitly time dependent reactive Hamiltonian, whose first contribution appears at 2.5PN order, is denoted by $H^{\rm r}_{\rm 2.5PN}$. In terms of the unscaled position and momentum vector components in the center-of-mass frame, and following Ref. [14], it reads

$$H^{\rm r}_{\rm 2.5PN} = \frac{2G}{5c^5}\frac{d^3 Q_{ij}}{dt^3}\left(\frac{p_i p_j}{\mu} - GM\mu\frac{r^i r^j}{r^3}\right)\,, \tag{24}$$

where $Q_{ij} = \mu\,(r_i r_j - r^2\,\delta_{ij}/3)$ stands for the Newtonian accurate mass-quadrupole of a compact binary. However, for the purpose of our investigation, it is convenient to consider the following physically equivalent reactive Hamiltonian at the 2.5PN order:

$$H^{\rm r}_{\rm 2.5PN} = \frac{G\mu}{5c^5}\frac{d^5 Q_{ij}}{dt^5} r^i r^j\,. \tag{25}$$

The above two reactive Hamiltonians differ by a total time derivative and thus belong to two different coordinate conditions [it is only for simplicity that dynamical variables are still denoted by same symbols in Eqs. (24) and (25)]. The reactive Hamiltonian given by Eq. (24) is valid under the ADM coordinate conditions, whereas Eq. (25) is for its counterpart in the Burke-Thorne gauge [16](notice that in the Burke-Thorne gauge, the reactive part of $h^{\rm TT}_{ij}$ is zero as explained in Ref. [17]). However, a change of coordinates at the reactive order, in comparison with the conservative part, does not influence any observable quantities.

With the help of Eq. (25), we define $\hat{\mathcal{H}}^{\rm r}_{\rm 2.5PN} = H^{\rm r}_{\rm 2.5PN}/\mu\,c^2$, and obtain, rather symbolically for the 2PN conservative part, the following fully 2.5PN accurate Hamiltonian equations of motion in polar coordinates and in dimensionless variables as

$$\frac{d\hat r}{d\hat t} = \frac{\partial \hat{\mathcal{H}}^{\rm c}_{\rm 2PN}}{\partial \hat p_r}\,, \tag{26a}$$

$$\frac{d\phi}{d\hat t} = \frac{\partial \hat{\mathcal{H}}^{\rm c}_{\rm 2PN}}{\partial \hat j} \equiv \hat\omega \tag{26b}$$

$$\frac{d\hat p_r}{d\hat t} = -\frac{\partial \hat{\mathcal{H}}^{\rm c}_{\rm 2PN}}{\partial \hat r} + f_{\hat p_r}\,, \tag{26c}$$

$$\frac{d\hat j}{d\hat t} = -\frac{\partial \hat{\mathcal{H}}^{\rm r}_{\rm 2.5PN}}{\partial \phi} \equiv f_{\hat j}\,, \tag{26d}$$

where $\hat{\mathcal{H}}^{\rm c}_{\rm 2PN} = H^{\rm c}_{\rm 2PN}/\mu\,c^2$ and the explicit expressions for $f_{\hat p_r}$ and $f_{\hat j}$ are given by

$$f_{\hat p_r} = \frac{16\,\eta\,\hat p_r}{15\,\hat r^5}\left\{4\,\hat r + 3\,\hat p_r^2 \hat r^2 + 18\,\hat j^2\right\}, \tag{27a}$$

$$f_{\hat j} = -\frac{8\,\eta\,\hat j}{5\,\hat r^5}\left\{-9\,\hat p_r^2 \hat r^2 + 6\,\hat j^2 - 2\,\hat r\right\}. \tag{27b}$$

As mentioned earlier, in this investigation we focus on black hole binaries inspiralling along quasi-circular orbits and we prescribe the quasi-circularity by imposing $\hat p_r \equiv 0$ on the reactive contributions to Hamiltonian equations of motion. This implies that Eqs. (27) becomes

$$f_{\hat p_r} \equiv 0\,, \tag{28a}$$

$$f_{\hat j} = -\frac{32}{5}\,\frac{\eta}{\hat r^{7/2}}\,. \tag{28b}$$

A close look at the above equation for $f_{\hat j}$ that defines $d\hat j/dt$ reveals that it is identical to the dominant contribution to the far-zone angular momentum flux associated with comparable mass binaries inspiralling along quasi-circular orbits. This observation helped us to provide the following prescription to incorporate radiation reaction on the conservative Skeleton Hamiltonian, given by Eqs. (22).

We recall that the Skeleton Hamiltonian providing the conservative part of the binary black hole dynamics is PN independent and therefore can be employed to treat close BBH configurations, provided we accept the validity of underlying assumptions. Therefore, in order to introduce gravitational radiation reaction effects, we invoke the most PN accurate expression for far-zone angular momentum flux associated with comparable mass compact binaries inspiralling along quasi-circular orbits to provide an evolution equation for $\hat j$. This is how we incorporate radiation reaction into Eqs. (22) and the dynamics it defines. The fully 3.5PN accurate expression for far-zone angular momentum flux for compact binaries in quasi-circular orbits, denoted by L_j and extractable from Ref. [5], reads

$$\begin{aligned} L_j = \frac{32}{5}\,\eta\,v^7 \Bigg\{ & 1 - \left[\frac{1247}{336} + \frac{35}{12}\,\eta\right] v^2 + 4\,\pi\,v^3 \\ & + \left[-\frac{44711}{9072} + \frac{9271}{504}\,\eta + \frac{65}{18}\,\eta^2\right] v^4 - \left[\frac{8191}{672}\right. \\ & \left. + \frac{583}{24}\,\eta\right] \pi\,v^5 + \left[\frac{6643739519}{69854400} + \frac{16}{3}\,\pi^2\right. \\ & - \frac{1712}{105}\,\gamma + \left(-\frac{134543}{7776} + \frac{41}{48}\,\pi^2\right)\eta - \frac{94403}{3024}\,\eta^2 \\ & \left. - \frac{775}{324}\,\eta^3 - \frac{1712}{105}\,\ln(4\,v)\right] v^6 + \left[-\frac{16285}{504}\right. \\ & \left. + \frac{214745}{1728}\,\eta + \frac{193385}{3024}\,\eta^2\right] \pi\,v^7 \Bigg\}\,, \end{aligned} \tag{29}$$

where $v \equiv \hat\omega^{1/3}$ and $\hat\omega = d\phi/d\hat t$ is the conservative dimensionless orbital frequency. The above equation is derived by noting that for circular orbits, the far-zone angular momentum and energy fluxes are related by $L_E = \omega L_j$.

Therefore, the Skeleton dynamics representing dynamics of comparable-mass non-spinning coalescing black hole binaries, in the scaled polar coordinates, can be summarized as

$$\frac{d\hat r}{d\hat t} = \frac{\partial \hat{\mathcal{H}}_{\rm Sk}}{\partial \hat p_r}\,, \tag{30a}$$

$$\frac{d\phi}{d\hat t} = \frac{\partial \hat{\mathcal{H}}_{\rm Sk}}{\partial \hat j} \equiv \hat\omega\,, \tag{30b}$$

$$\frac{d\hat p_r}{d\hat t} = -\frac{\partial \hat{\mathcal{H}}_{\rm Sk}}{\partial \hat r}\,, \tag{30c}$$

$$\frac{d\hat j}{d\hat t} = -L_j\,, \tag{30d}$$

where L_j, the 3.5PN accurate far-zone angular momentum flux, is given by Eq. (29). It is important to note that, in our prescription, $\hat\omega$ appearing in the PN accurate expression for L_j via $v \equiv \hat{\omega}^{1/3}$ is provided by the Skeleton dynamics [in other words, by Eq. (30b)]. The computational details required to compute right hand sides of Eqs. (30) are provided in the Appendix A

We have already argued that the Skeleton Hamiltonian, given by Eq. (22), does provide a certain conservative dynamics for two punctures orbiting each other. Therefore, Eqs. (30) represent a prescription to implement semi-analytically puncture evolution to model merging binary black holes with reasonable precision. It should be noted that the use of Eq. (29) implies that the adiabatic inspiral occurs along quasi-circular orbits.

We observe that the arguments that allowed us to employ PN accurate far-zone angular momentum flux to incorporate the effects of radiation reaction into our conservative (and PN independent) Hamiltonian is fairly elegant compared to somewhat heuristic arguments employed by the advocates of the EOB scheme (see Sec. III in Ref. [18]). Further, the EOB approach usually requires re-summed Padé estimates for $d\hat{j}/d\hat{t}$ that also require PN accurate far-zone angular momentum flux, to include effects of radiation reaction on the conservative EOB Hamiltonian. We have experimented with various Padé estimates for $d\hat{j}/d\hat{t}$ in our Skeletonian approach. However, the final value of the Skeletonian $\hat{j}$, when $\hat{\omega}$ reaches its maximum value, turned out to be rather insensitive to the choice of Padé or Taylor approximant for $d\hat{j}/d\hat{t}$. Therefore, in this paper, we employed only the usual 3.5PN (Taylor) accurate expression for far-zone angular momentum flux, in terms of $v \equiv \hat{\omega}^{1/3}$, given by Eq. (29).

In the next section, we describe how we numerically implement the reactive Skeleton dynamics and explore its various facets.

III. NUMERICAL EXPLORATION OF REACTIVE SKELETON DYNAMICS

Let us first detail how we provide initial conditions required to define $\hat{\mathcal{H}}_{\rm Sk}$ and to solve Eqs. (30).

A. Initial conditions required to define reactive Skeleton dynamics

It is obvious that the equations describing the late stages of binary black hole dynamics, given by Eqs. (30), require us to specify $\hat{\mathcal{H}}_{\rm Sk}$ defined in terms of $\psi_1(\psi_2, \hat{r}, \hat{p}_r, \hat{j})$ and $\psi_2(\psi_1, \hat{r}, \hat{p}_r, \hat{j})$. This implies that we need to find ways to specify values for $\hat{r}, \phi, \hat{p}_r, \hat{j}, \psi_1$ and ψ_2 at an initial instant, say $t = 0$. The initial conditions for $\hat{r}$ and ϕ are arbitrary and specify the initial radial separation and its associated angular position.

The 2PN accurate expression for $\hat{p}_r$ in terms of $\hat{r}$ in the ADM coordinates, displayed below, is our initial condition for $\hat{p}_r$

$$\hat{p}_r = -\frac{64}{5}\frac{\eta}{\hat{r}^3} + \left(\frac{460}{21}\frac{\eta}{\hat{r}^4} + 16\frac{\eta^2}{\hat{r}^4}\right) - \frac{256}{5}\frac{\eta\,\pi}{\hat{r}^{9/2}} + \left(-\frac{1568}{45}\frac{\eta^2}{\hat{r}^5} - \frac{158224}{2835}\frac{\eta}{\hat{r}^5}\right). \tag{31}$$

The derivation of Eq. (31) requires following inputs and is done in three steps. First, we compute $d\hat{r}/d\hat{t}$ associated with the quasi-circular inspiral to 2PN order with the help of Ref. [5]. Employing the 2PN accurate relation connecting $\hat{j}$ and $\hat{r}$, relevant for PN accurate circular orbits, we iterate the 2PN accurate Hamiltonian Equation for symbolically $d\hat{r}/d\hat{t}$, written in terms of $\hat{r}, \hat{p}_r$ and $\hat{j}$, and compute $\hat{p}_r$ as a PN accurate polynomial in $d\hat{r}/d\hat{t}$. In the final step, we invoke $d\hat{r}/d\hat{t}$, accurate to 2PN radiation reaction order (and was computed in the first step) and obtain PN accurate expression for $\hat{p}_r$ in terms of $\hat{r}$, given by Eq. (31).

The initial value for $\hat{j}$ is computed by solving $d\hat{p}_r/d\hat{t} = 0$, where $d\hat{p}_r/d\hat{t}$ is given by Eq. (30c). It should be obvious that we need to specify r, p_r, ψ_1 and ψ_2 to obtain numerically the value for $\hat{j}$ by imposing the right hand side of Eq. (30c) to zero. We provide initial guesses for ψ_1 and ψ_2 by invoking the ingredients used to construct Brill-Lindquist potential function, associated with the Brill-Lindquist initial value solution for two black holes at rest [11]. This leads to the following expressions for ψ_1 and ψ_2 in terms of $\hat{r}$ and η:

$$\psi_1^{\rm BL} = \frac{1}{2} - \frac{\sqrt{1-4\,\eta}}{4\,\hat{r}} + \frac{1}{2}\sqrt{1 + \frac{1}{\hat{r}} + \frac{1}{4\,\hat{r}^2} - \frac{\eta}{\hat{r}^2}}\,, \tag{32a}$$

$$\psi_2^{\rm BL} = \frac{1}{2} + \frac{\sqrt{1-4\,\eta}}{4\,\hat{r}} + \frac{1}{2}\sqrt{1 + \frac{1}{\hat{r}} + \frac{1}{4\,\hat{r}^2} - \frac{\eta}{\hat{r}^2}}\,. \tag{32b}$$

We would like to emphasize that it is only during the evaluation of an initial guess for $\hat{j}$ that we invoke Eqs. (32). Further, while performing various checks, we realized that the initial value of $\hat{j}$ is rather insensitive to the choice of $\hat{p}_r$. In other words, initial value for $\hat{j}$ does not change much even when we use $\hat{p}_r = 0$ on the right hand side of Eq. (30c).

We are now in a position to obtain initial values for ψ_1 and ψ_2 that are required to solve Eqs. (30). The initial values for ψ_1 and ψ_2, associated with the above mentioned $\hat{r}, \hat{p}_r$ and $\hat{j}$ values are numerically evaluated using the coupled algebraic equations for ψ_1 and ψ_2, given in Eqs. (22).

From here onwards, we drop *hat symbol* appearing on our dimensionless quantities like $\hat{\mathcal{H}}_{\rm Sk}, \hat{r}, \hat{p}_r, \hat{j}, \hat{\omega}, \hat{t}$ for the ease of presentation.

B. Various aspects of the reactive Skeleton binary black hole dynamics

Before we probe numerically the various aspects of the SAPE to model merging binary black holes, having

$\eta = 1/4$, let us state that the way of solving Eqs. (30) is quite different from the way one solves Hamiltonian equations when the Hamiltonian is explicitly given in terms of r, p_r and j. While dealing with the reactive 2.5PN accurate Hamiltonian system, given by Eqs. (26), or the EOB scheme, one needs to invoke *only once* a numerical scheme, like the 4th order Runge-Kutta, to solve the associated couple differential equations, after specifying certain initial conditions for r, p_r and j. However, a similar approach is not applicable for the reactive Skeleton dynamics, given by Eqs. (30) . This is because of the fact that the Skeleton Hamiltonian, given by Eq. (22), implicitly depends on r, p_r and j and its explicit dependence on ψ_1 and ψ_2 is interconnected. Therefore, the numerical solution to Eqs. (30) is determined in the following way. We have already detailed how to prescribe initial values for r, ϕ, p_r, j, ψ_1 and ψ_2 in the previous subsection. With the aid of these initial guesses, we invoke the 4th order Runge-Kutta to solve Eqs. (30) and obtain values for r, p_r, ϕ and j at the next time step δt. These values are employed to evaluate the values of ψ_1 and ψ_2 at the instant δt, with the help of the coupled algebraic equations for ψ_1 and ψ_2, given in Eqs. (22). To obtain the values of the dynamical variables at the next instant, $2\delta t$, we use as initial guesses, the values of r, p_r, ϕ, j, ψ_1 and ψ_2 at the earlier step, and repeat the above detailed procedure all over again till we reach the terminal point of our evolution. This is how we obtain numerical solution to the reactive Skeleton dynamics for binary black hole evolution, given by Eqs. (30). In other words, we need to call the 4th order Runge-Kutta at every time step t to obtain the values of r, p_r, ϕ, j, ψ_1 and ψ_2 at $t + \delta t$. However, while solving the 2.5PN accurate Hamiltonian equations, Eqs. (26) or the EOB differential equations, one usually invokes a numerical scheme like the 4th order Runge-Kutta only once.

We are now in a position to extract (numerically) various aspects of the reactive Skeleton dynamics for binary black hole evolution. In this paper, we terminate the SAPE when $\omega(t)$ reaches its maximum value, $\omega_{\rm mx}$ and let the initial value for r to be 10. Plots depicting temporal evolutions of various dynamical variables, appearing in Eqs. (30), for a binary black hole having $\eta = 0.25$ is presented in Fig. 1. The parametric plot of $x = r\cos\phi$ versus $y = r\sin\phi$ clearly indicates that the dynamical evolution, predicted by Eqs. (30), occurs along inspiralling quasi-circular orbits and it is rather difficult to pin-point the position of the last stable orbit, which can clearly be defined using the conservative Skeleton Hamiltonian as done in Ref. [8]. Further, we observe that both the binding energy, given by the Skeleton Hamiltonian, and j, the orbital angular momentum vary smoothly till we terminate the reactive Skeleton evolution at $\omega = \omega_{\rm mx} \sim 0.0896$. The temporal behavior of p_r clearly indicates that even in the neighborhood of $\omega_{\rm mx}$, the orbital motion is not substantially different from a quasi-circular inspiral. The region where p_r increases sharply may considered to be the plunge phase. In Fig. 2, we explore $r(t), \omega(t)$ and $\dot{r}^2(t)$ under reactive Skeleton dynamics. Plots of ω versus t and ω versus r indicate faster evolution for ω after the late inspiral stage. The rapid decrease in r during the plunge phase is also evident in the r versus t plot. Interestingly, $\dot{r}^2 = (dr/dt)^2$ remains small even during the plunge phase. However, it changes from $\sim 10^{-3}$ to $\sim 10^{-2}$ when t changes from ~ 588 to ~ 627, which clearly indicate deviations from the adiabatic evolution along circular orbits of decreasing radii, expected during the quasi-circular inspiral. Another interesting aspect of the SAPE is that the reactive evolution becomes slightly eccentric if we choose $p_r \equiv 0$ at the initial instant $t = 0$ and this is also displayed in Fig. 2. We would like to point out that residual eccentricities appearing in the puncture evolution in full General Relativity were suppressed in a similar manner in Ref. [19].

The nature of the BBH evolution during the plunge phase, predicted by Eqs. (30) is probed in Fig. 3. First, we plot the $\omega^2\, r^3$, the 'Kepler combination', against r. This plot is motivated by the observation in Ref. [7] that for the reactive EOB evolution $\omega^2\, r^3$, which remains close to unity during the quasi-circular inspiral, decreases rapidly during the plunge. We note that, similar to what is observed in the Numerical Relativity based evolution of punctures, the 'Kepler combination' varies even during the inspiral. Therefore, it is reasonable to state that the constancy of 'Kepler combination', observed in Ref. [7], is purely a consequence of the fact that the EOB scheme employs Schwarzschild-like coordinates. In Fig. 3, we also plot $v_\omega^2 \equiv \omega^{2/3}$ versus t and $v_{\rm G}^2 \equiv r^2\,\omega^2 + \dot{r}^2$ versus t and observe that v_ω remains larger than $v_{\rm G}$ throughout the Skeleton inspired inspiral. The above two plots indicate that in reactive Skeleton dynamics, it is not very attractive to employ $v = r\,\omega$ or $v = v_{\rm G}$ in the expression for the far-zone angular momentum flux while incorporating radiation reaction on the conservative Skeleton dynamics. A plot of the 'quasi-circularity' condition $dE = \bar{\omega} dj$, valid for binary inspirals along a sequence of circular orbits is also available in Fig. 3. The quantities dE and dj represent differences in the values of $\mathcal{H}_{\rm Sk}$ and j at t and $t + \delta t$, while $\bar{\omega}$ is the average value of ω, given by Eq. (30b), at t and $t + \delta t$. We observe that the degree with which the above relation is violated keeps getting bigger as we approach $\omega_{\rm mx}$. However, the difference between dE and $\bar{\omega}\, dj$ is small even in the neighborhood of $\omega_{\rm mx}$ indicating that the plunge motion is fairly close to 'quasi-circular'. Therefore, in our opinion, the plots in Fig. 3 suggest that it is not very unrealistic to employ v_ω to estimate the effects of radiation reaction in our SAPE.

Let us perform a first-order comparison between the GW phase evolutions based on SAPE and Numerical Relativity (NR) for an equal mass binary during its late inspiral without using any data from NR simulations. This is possible due to the observation, reported in Ref. [20], that GW phase evolution associated with certain PN approximant, namely TaylorT4 at 3.5PN order, closely agrees with equal mass binary black hole NR simulations that last around 15 orbits prior to the merger[the accumulated phase difference is less than 0.05 radians over the 30-cycle waveform]. The orbital phase evolution for equal mass binary black holes under TaylorT4 approximant at 3.5PN order is obtained by numerically integrating the following two differential equations [20]:

$$\frac{d\phi(t)}{dt} \equiv x^{3/2}\,, \tag{33a}$$

$$\begin{aligned}\frac{d\,x(t)}{dt} &= \frac{16}{5}\,x^5 \bigg\{ 1 - \frac{487}{168}\,x + 4\,\pi\,x^{3/2} \\ &+ \frac{274229}{72576}\,x^2 - \frac{254}{21}\,\pi\,x^{5/2} \\ &+ \bigg[\frac{178384023737}{3353011200} - \frac{1712}{105}\,\gamma + \frac{1475}{192}\,\pi^2 \\ &- \frac{856}{105}\,\ln\left(16\,x\right) \bigg] x^3 + \frac{3310}{189}\,\pi\,x^{7/2} \bigg\}\,,\end{aligned} \tag{33b}$$

where γ is the Euler gamma and $x = \omega^{2/3}$. In what follows, we compare the orbital phase evolution prescribed by SAPE for $\eta = 0.25$ with $\phi(t)$ originating from Eq. (33).

There are two slightly different ways to compare $\phi_{\rm Sk}(t)$ against $\phi_{\rm T4}(t)$ after choosing a specific interval for x, defined by some minimum and maximum values, say $x_{\rm min}$ and $x_{\rm max}$, for x. In the first approach, one lines up $\phi_{\rm Sk}(t), \phi_{\rm T4}(t)$ and their time derivatives at $x = x_{\rm max}$ and with the help of a shifted $\phi_{\rm T4'}(t)$, given by Eq. (49) in Ref. [20], computes $\phi_{\rm Sk}(t) - \phi_{\rm T4'}(t)$ when $x = x_{\rm min}$ [this is pursued in Refs. [21]]. In the second prescription, one lines up $\phi_{\rm Sk}(t), \phi_{\rm T4}(t)$ and their time derivatives at $x = x_{\rm min}$ and computes $\phi_{\rm Sk}(t) - \phi_{\rm T4}(t)$ when x reaches $x_{\rm max}$ and this is what we list below and the differences between the two prescriptions in our comparisons are always negligible. In Fig. 4, we plot $\phi_{\rm Sk}(t) - \phi_{\rm T4}(t)$ in radians and $x(t)$ under SAPE and T4 approximant at 3.5PN order for various x intervals. For the top panel, the orbital frequency range is from $\omega = 0.025$ to $\omega = 0,05$ and there are ~ 8.5 cycles. In the middle panel, we vary ω from 0.025 to 0.045 and there are about 8 cycles. Finally, for the bottom panel there are about 11.5 cycles and the ω interval is from 0.0222 to 0.045. Further, the fractional differences in ϕ are $\sim 7\%, 5.8\%$ and $\sim 6.1\%$ in the above three cases and it increase sharply as we approach the plunge.

It should be emphasized that we haven't employed any arbitrary parameters in our SAPE. Therefore, it is conceivable that by introducing flexible parameters, we should be able to obtain a modified reactive Skeletonian dynamics that prevents the above observed dephasing. This is inspired by what is advised in the modified EOB approach [4] and it will be reported in a separate publication.

IV. ROUGH PRESCRIPTION TO OBTAIN BBH COALESCENCE WAVEFORMS VIA SAPE

We aim to provide, in this section, a rough estimate for the GW polarizations, having Newtonian accurate amplitude, associated with the BBH coalescence in our SAPE. This is achieved by terminating the SAPE when ω, given by Eq. (30b), reaches its maximum value $\omega_{\rm mx}$ an then matching there the relevant time derivatives of the radiative multipole moments associated with the late plunge phase to the corresponding 'ring-down' multipole moments, constructed using appropriate quasi-normal mode(QNM) contributions. Our construction of $h^{\rm N}_{\times}(t)$ and $h^{\rm N}_{+}(t)$, *i.e.* the temporally evolving GW polarizations having Newtonian accurate amplitude, for the ring-down phase after the termination of the SAPE follows very closely what is detailed Sec. IV of Ref. [7].

The GW polarizations are defined in the following way

$$h_\times = h^{\rm TT}_{\hat{\boldsymbol\theta}\,\hat{\boldsymbol\phi}}\,, \tag{34a}$$

$$h_+ = \frac{1}{2}\left(h^{\rm TT}_{\hat{\boldsymbol\theta}\,\hat{\boldsymbol\theta}} - h^{\rm TT}_{\hat{\boldsymbol\phi}\,\hat{\boldsymbol\phi}} \right)\,, \tag{34b}$$

where $h^{\rm TT}_{\hat{\boldsymbol\theta}\,\hat{\boldsymbol\phi}}$ and $h^{\rm TT}_{\hat{\boldsymbol\theta}\,\hat{\boldsymbol\theta}}$ are the independent components of $h^{\rm TT}_{ij}$ representing the radiation field emitted by isolated systems in asymptomatically flat space-time. The various angular components of $h^{\rm TT}_{ij}$ are defined using a spherical coordinate system, having orthonormal bases $(\hat{\boldsymbol r}', \hat{\boldsymbol\theta}, \hat{\boldsymbol\phi})$, centered on the center-of-mass of the binary and whose azimuthal axis is aligned with the orbital angular momentum vector $\boldsymbol l$. Following Ref. [22], it is possible to obtain $h^{\rm TT}_{ij}$ in terms of certain time derivatives of the radiative mass and current moments $\mathcal{I}^{lm}$ and $\mathcal{S}^{lm}$, irreducibly defined with respect to $\boldsymbol l$, where $m = -l, -l{+}1, .., +l$ and $T^{\rm E2,lm}_{ij}$ and $T^{\rm B2,lm}_{ij}$: the so-called pure-spin tensor-spherical harmonics of electric and magnetic types. To compute $h^{\rm N}_{\times,+}$, we only require dominant contributions to $h^{\rm TT}_{ij}$ given by

$$h^{\rm TT}_{ij}|_{\rm N} = \frac{G}{c^4\,r'} \sum_{m=-2}^{2} {}^{(2)}\mathcal{I}^{2m}(t - r'/c)\,T^{\rm E2,2m}_{ij}\,. \tag{35}$$

It turns out that at the Newtonian order, $\mathcal{I}^{20} = \mathcal{I}^{21} \equiv 0$ and contributions arising from $m = -2$ are evaluated using the usual relation $\mathcal{I}^{2-2} = \mathcal{I}^{2+2^*}$, where $*$ stands for complex conjugation. Therefore, only the following expressions are required to compute $h^{\rm N}_{\times,+}$

$${}^{(2)}\mathcal{I}^{22} = -\frac{8}{5}\,\sqrt{10\,\pi}\,\eta\,m\,c^2\,\omega^{2/3}\,e^{-2\,i\,\phi(t)}\,, \tag{36a}$$

$$\begin{aligned} T^{\rm E2,22} &= \left(\frac{5}{128\,\pi}\right)^{1/2} e^{2\,i\,\varphi} \bigg\{ \bigg[(1 + \cos\vartheta^2) \bigg(\hat{\boldsymbol\theta} \otimes \hat{\boldsymbol\theta} \\ &- \hat{\boldsymbol\phi} \otimes \hat{\boldsymbol\phi} \bigg) + 2\,i\,\cos\vartheta \bigg(\hat{\boldsymbol\theta} \otimes \hat{\boldsymbol\phi} + \hat{\boldsymbol\phi} \otimes \hat{\boldsymbol\theta} \bigg\}\,. \end{aligned} \tag{36b}$$

With these inputs, we obtain

$$h^{\rm N}_\times = -4\,\eta\,\cos i\,\left(\frac{G\,m}{c^2\,r'}\right)\,\omega^{2/3}\,\sin 2\,\phi\,, \tag{37a}$$

$$h^{\rm N}_+ = -2\,\eta\,\left(1 + \cos^2 i\right)\,\left(\frac{G\,m}{c^2\,r'}\right)\,\omega^{2/3}\,\cos 2\,\phi\,, \tag{37b}$$

where we identified $\vartheta = i$, the orbital inclination angle and set $\varphi = 0$.

Following Ref. [7], we aim to match as smooth as possible ${}^{(2)}\mathcal{I}^{2\pm2}_{\rm plunge}$, given in Eqs. (36), at $t = t_{\rm m}$, $t_{\rm m}$ being the time when the SAPE $\omega(t)$ reaches its maximum value, to the corresponding ring-down ${}^{(2)}\mathcal{I}^{2\pm2}_{\rm ring}$ consisting of certain sum of decaying QNM modes. For simplicity, we restrict our attention to ${}^{(2)}\mathcal{I}^{2\pm2}_{\rm ring}$ constructed using the first two complex conjugated fundamental QNM modes. For this purpose, we only need to know the following conjugate pair of complex QNM frequencies, extractable from Ref. [23],

$$\sigma_{20}^{\pm} = 0.08896 \pm 0.37367\, i\,. \tag{38}$$

Under these restrictions, ${}^{(2)}\mathcal{I}^{2\pm2}$ during the ring-down phase is given by

$$\begin{aligned} {}^{(2)}\mathcal{I}^{2+2}_{\rm ring} &= C_0^{+}\, e^{-\sigma_{20}^{+}\,\tau} + C_0^{-}\, e^{-\sigma_{20}^{-}\,\tau} \\ &\qquad (\text{for } \ \tau \equiv t - t_{\rm m} > 0) \end{aligned} \tag{39}$$

The two arbitrary complex coefficients $C_0^{+}(\mathcal{I}^{22})$ and $C_0^{-}(\mathcal{I}^{22})$ can be chosen so as to ensure not only that ${}^{(2)}\mathcal{I}^{22}_{\rm plunge}(t = t_{\rm m})$ agrees with ${}^{(2)}\mathcal{I}^{22}_{\rm ring}(t = t_{\rm m}) = C_0^{+}(\mathcal{I}^{22}) + C_0^{-}(\mathcal{I}^{22})$, but also that the numerically computed time derivative of ${}^{(2)}\mathcal{I}^{22}_{\rm plunge}(t)$, *i.e.* ${}^{(3)}\mathcal{I}^{22}_{\rm plunge}(t)$ agrees, when $t = t_{\rm m}$ with ${}^{(3)}\mathcal{I}^{22}_{\rm ring} = -\sigma_{20}^{+}\, C_0^{+}(\mathcal{I}^{22}) - \sigma_{20}^{-}\, C_0^{-}(\mathcal{I}^{22})$. This yields

$$C_0^{+}(\mathcal{I}^{22}) = \left(\sigma_{20}^{-} - \sigma_{20}^{+}\right)^{-1} \Bigg[\sigma_{20}^{-}\, {}^{(3)}\mathcal{I}^{22}_{\rm plunge}(t) + {}^{(4)}\, \mathcal{I}^{22}_{\rm plunge}(t)\Bigg]_{t=t_{\rm m}} \tag{40a}$$

$$C_0^{-}(\mathcal{I}^{22}) = \left(\sigma_{20}^{+} - \sigma_{20}^{-}\right)^{-1} \times \Bigg[\sigma_{20}^{+}\, {}^{(3)}\mathcal{I}^{22}_{\rm plunge}(t) + {}^{(4)}\, \mathcal{I}^{22}_{\rm plunge}(t)\Bigg]_{t=t_{\rm m}} \tag{40b}$$

We would like to point out that while computing ${}^{(3)}\mathcal{I}^{2+2}_{\rm plunge}(t)$, we include the $d\omega/dt$ contribution, with the help of Eqs. (A2). Using the above detailed prescriptions for ${}^{(2)}\mathcal{I}^{2+2}_{\rm ring}$, it is now fairly straightforward to obtain $h^{\rm N}_{\times,+}$ associated with BBH coalescence under SAPE that also includes contributions from QNM ringing phase.

In Numerical Relativity, it is customary to invoke the Weyl scalar ψ_4 to represent the gravitational wave content of the dynamical space-time. In a suitable null tetrad and in the far-zone, one finds

$$\psi_4 = \ddot{h}_{+} - i\, \ddot{h}_{\times}\,. \tag{41}$$

The $\Re(\psi_4)$ and $\Im(\psi_4)$ having 'Newtonian' amplitude, similar to Eqs. (37) read

$$\Re(\psi_4) = -8\, \left(1 + \cos i^2\,\right) \left(\frac{G\, m}{c^2\, r'}\right) \eta\, \omega(t)^{8/3}\, \cos 2\,\phi(t)\,, \tag{42a}$$

$$\Im(\psi_4) = -16\, \cos i \left(\frac{G\, m}{c^2\, r'}\right) \eta\, \omega(t)^{8/3}\, \sin 2\,\phi(t)\,. \tag{42b}$$

The resulting plots for $h^{\rm N}_{\times,+}(t)$ and the associated $\Re(\psi_4)$ and $\Im(\psi_4)$ are displayed in Fig. 5. The plots clearly demonstrate a smooth matching to the QNM ringing phase in the SAPE.

V. DISCUSSION AND FUTURE DIRECTIONS

This paper provides a semi-analytic prescription to model the BBH coalescence where we employ the punctures, employed by several Numerical Relativity groups, to model the non-spinning black holes. Our approach requires the conservative Skeleton Hamiltonian, derived in Ref. [8], representing two orbiting punctures in a waveless truncation to the Einstein field equations. We include the effects of radiation reaction in a transparent Hamiltonian framework that fully justifies the physical system we are trying to model. This is how we provide a prescription to implement our semi-analytic puncture evolution, termed SAPE, to model the merging binary black-holes. We also provided GW polarizations, real and imaginary parts of the Weyl scalar, having Newtonian amplitude, associated with the entire BBH coalescence in our SAPE. This is achieved by matching smoothly ${}^{(2)}\mathcal{I}^{2\pm2}_{\rm plunge}(t)$, when $\omega = \omega_{\rm mx}$, to ${}^{(2)}\mathcal{I}^{2\pm2}_{\rm ring}(t)$, constructed with the dominant black hole quasi-normal modes. We observe that Eqs. (30) defining our semi-analytic puncture evolution display features and predictions qualitatively similar to what are observed by various Numerical Relativity groups employing punctures to model black-holes.

Efforts are being planned to compare the predictions of a suitably modified SAPE with that arising from the modified EOB approach. We have also initiated a program to include the spin effects into $\mathcal{H}_{\rm Sk}$. Further, due to the fact that $\mathcal{H}_{\rm Sk}$ is exact while describing the motion of a test black hole in the Schwarzschild spacetime, a refined version of the SAPE should be of some interest to GW physicists, excited by the prospect of LISA observing Extreme/Intermediate Mass Ratio Inspirals.

Acknowledgments

It is our pleasure to thank Mark Hannam for discussions. This work is supported in part by the DFG (Deutsche Forschungsgemeinschaft) through SFB/TR7 "Gravitationswellenastronomie" and the DLR (Deutsches Zentrum für Luft- und Raumfahrt).

APPENDIX A: FORMULAE REQUIRED TO IMPLEMENT RIGHT HAND SIDES OF EQS. (30)

A close inspection of Eq. (22) reveals that $\mathcal{H}_{\rm Sk}$ depends implicitly on r, p_r and j. Therefore, evaluating right hand sides of Eqs. (30) in the SAPE is rather involved. Using the theorem of implicit differentiation, $\partial\mathcal{H}_{\rm Sk}/\partial p_r$ may be computed using the following relation

$$\left.\frac{\partial\psi_2}{\partial p_r}\right|_{r,j\ \rm fixed} = \left\{\frac{\partial\psi_2}{\partial p_r} + \left(\frac{\partial\psi_2}{\partial\psi_1}\right)\times\left(\frac{\partial\psi_1}{\partial p_r}\right)\right\}\Big/\left\{1-\left(\frac{\partial\psi_1}{\partial\psi_2}\right)\times\left(\frac{\partial\psi_2}{\partial\psi_1}\right)\right\}, \tag{A1}$$

and a similar relation holds for $\frac{\partial\psi_1}{\partial p_r}$. We follow a similar scheme to compute the right hand sides of equations that define $d\phi/dt$ and dp_r/dt.

During our matching to the QNMs, we require to compute ${}^{(3)}\mathcal{I}^{22}_{\rm plunge}(t)$ and this demands computation of $d\omega/dt$ under the SAPE. From Eq. (30b), it is clear that $\dot\omega$ requires us to compute $d\psi_1/dt$ and $d\psi_2/dt$ and we use following relations:

$$\frac{d\psi_1}{dt} = \left\{\left(\frac{\partial\psi_1}{\partial\psi_2}\right)\kappa_2+\kappa_1\right\}\Big/\left\{1-\left(\frac{\partial\psi_1}{\partial\psi_2}\right)\times\left(\frac{\partial\psi_2}{\partial\psi_1}\right)\right\}, \tag{A2a}$$

$$\frac{d\psi_2}{dt} = \left\{\left(\frac{\partial\psi_2}{\partial\psi_1}\right)\kappa_1+\kappa_2\right\}\Big/\left\{1-\left(\frac{\partial\psi_1}{\partial\psi_2}\right)\times\left(\frac{\partial\psi_2}{\partial\psi_1}\right)\right\},\ \text{where} \tag{A2b}$$

$$\kappa_1 = \left(\frac{\partial\psi_1}{\partial r}\right)\frac{dr}{dt}+\left(\frac{\partial\psi_1}{\partial p_r}\right)\frac{dp_r}{dt}+\left(\frac{\partial\psi_1}{\partial j}\right)\frac{dj}{dt}, \tag{A2c}$$

$$\kappa_2 = \left(\frac{\partial\psi_2}{\partial r}\right)\frac{dr}{dt}+\left(\frac{\partial\psi_2}{\partial p_r}\right)\frac{dp_r}{dt}+\left(\frac{\partial\psi_2}{\partial j}\right)\frac{dj}{dt}. \tag{A2d}$$

We would like to emphasize Eqs. (A2) are only required during our matching to the QNMs.

[1] F. Pretorius, Phys. Rev. Lett. **95**, 121101 (2005); M. Campanelli *et al.*; Phys. Rev. Lett. Phys. Rev. Lett. **96**, 111101 (2006); J. Baker *et al.*; Phys. Rev. Lett. **96**, 111102 (2006); B. Brügmann *et al.*; arXiv:gr-qc/0610128; M. Boyle *et al.*, arXiv:0710.0158 [gr-qc]; L. Rezzolla *et al.*, arXiv:0712.3541.

[2] L. E. Kidder, C. M. Will and A. G. Wiseman, Class. Quant. Grav. **9**, L127 (1992); Phys. Rev. D **47**, 3281 (1993).

[3] A. Buonanno and T. Damour, Phys. Rev. D **59**, 084006 (1999); Phys. Rev. D **62**, 064015 (2000); T. Damour, P. Jaranowski, and G. Schäfer, Phys. Rev. D **62**, 084011 (2000); T. Damour, Phys. Rev. D **64**, 124013 (2001); A. Buonanno, Y. Chen, and T. Damour, gr-qc/0508067.

[4] T. Damour, arXiv:0802.4047[gr-qc] and related references therein.

[5] T. Damour, P. Jaranowski, and G. Schäfer, Phys. Lett. B **513**, 147 (2001); L. Blanchet, G. Faye, B. R. Iyer, and B. Joguet, Phys. Rev. D **65**, 061501(R) (2002); **71**, 129903(E) (2005); L. Blanchet, T. Damour, G. Esposito-Farèse, and B. R. Iyer, Phys. Rev. Lett. **93**, 091101 (2004) and references therein.

[6] N. Wex and G. Schäfer, Class. Quant. Grav. **10**, 2729 (1993).

[7] T. Damour and A. Gopakumar, Phys. Rev. D **73**, 124006 (2006)

[8] G. Faye, P. Jaranowski and G. Schäfer Phys. Rev. D **69**, 124029 (2004) [arXiv:gr-qc/0311018].

[9] R. Arnowitt, S. Deser and C. W. Misner, *The Dynamics of General Relativity.* In *Gravitation: An Introduction to Current Research*, ed. by L. Witten (John Wiley, New York 1962) p. 227[arXiv:gr-qc/0405109].

[10] D. R. Brill and R. W. Lindquist, Phys. Rev. **131**, 471 (1963).

[11] P. Jaranowski and G. Schäfer, Phys. Rev. D **60**, 124003 (1999) [arXiv:gr-qc/9906092]; Phys. Rev. D **65**, 127501 (2002) [arXiv:gr-qc/0202035].

[12] A. Komar Phys. Rev. **113**, 934 (1959).

[13] S. Brandt and B. Brügmann, Phys. Rev. Lett. **78**, 3606 (1997).

[14] G. Schäfer, Astronomische Nachrichten **311**, 213 (1990); in *Symposia Gaussiana*, Proceedings of the 2nd Gauss Symposium, Conference A: Mathematics and Theoretical Physics, edited by M. Behara, R. Fritsch and R. Lintz (Walter de Gruyter, Berlin) 667 (1995).

[15] T. Damour and G. Schäfer, Nuovo Cimento B **101**, 127 (1988).

[16] C. W. Misner, K. S. Thorne, and J. A. Wheeler, *Gravitation* (Freeman, San Francisco, 1973) paragraph 36.8.

[17] G. Schäfer, Lettere Al Nuovo Cimento **36**, 105 (1983).

[18] A. Buonanno and T. Damour, Phys. Rev. D **62**, 064015 (2000).
[19] S. Husa, M. Hannam, J. A. Gonzalez, U. Sperhake and B. Brügmann, arXiv:0706.0904 [gr-qc].
[20] M. Boyle *et al.*, arXiv:0710.0158 [gr-qc]
[21] J. G. Baker *et al.*, Phys. Rev. Lett. **99**, 181101 (2007); M. Hannam, *et al.*, arXiv:0706.1305[gr-qc]; A. Gopakumar, *et al.*, arXiv:0712.3737 [gr-qc].
[22] K. S. Thorne, Rev. Mod. Phys. **52**, 299 (1980); W. Junker and G. Schäfer, Mon. Not. R. Astron. Soc. **254**, 146 (1992).
[23] K. D. Kokkotas, and S. Schmidt "Quasi-Normal Modes of Stars and Black Holes", Living Rev. Relativity **2**, 2 (1999).

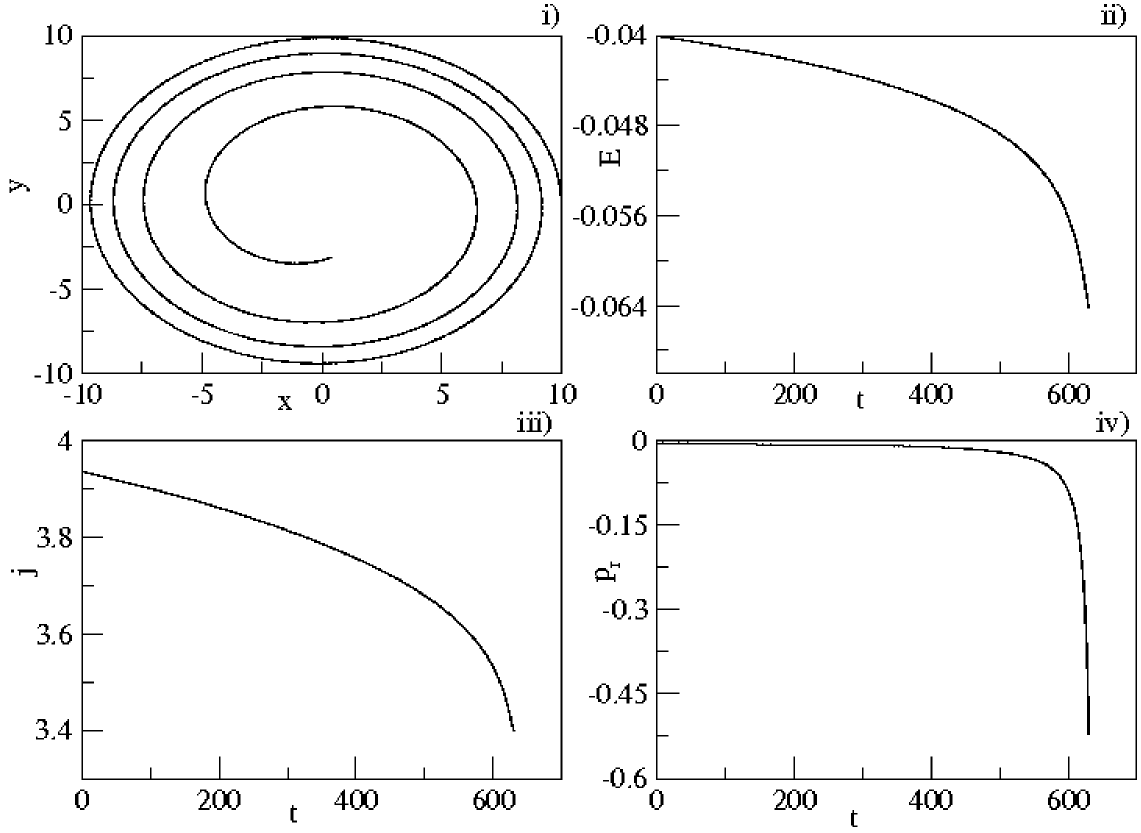

FIG. 1: Plots depicting various facets of SAPE, defined by Eqs. (30), for a $\eta = 0.25$ BBH having initial orbital separation $r = 10$ [recall that we have dropped *hat symbol* appearing in the dimensionless variables defined by Eq. (21)]. In these plots, we terminate the SAPE when ω reaches its maximum value, $\omega_{\rm mx} \sim 0.0896$. The Panel (i) provides a parametric plot of $x = r\,\cos\phi$ versus $y = r\,\sin\phi$, indicating that the SAPE occurs along quasi-circular orbits. The temporal evolutions for the dimensionless binding energy, $E \equiv \mathcal{H}_{\rm Sk}$, and the orbital angular momentum j are plotted in the panels (ii) and (iii). The plot for $p_r(t)$ suggests that even during the dynamical plunge, *i.e.* in the neighborhood of $\omega_{\rm mx}$, the orbital motion is not that different from a quasi-circular inspiral.

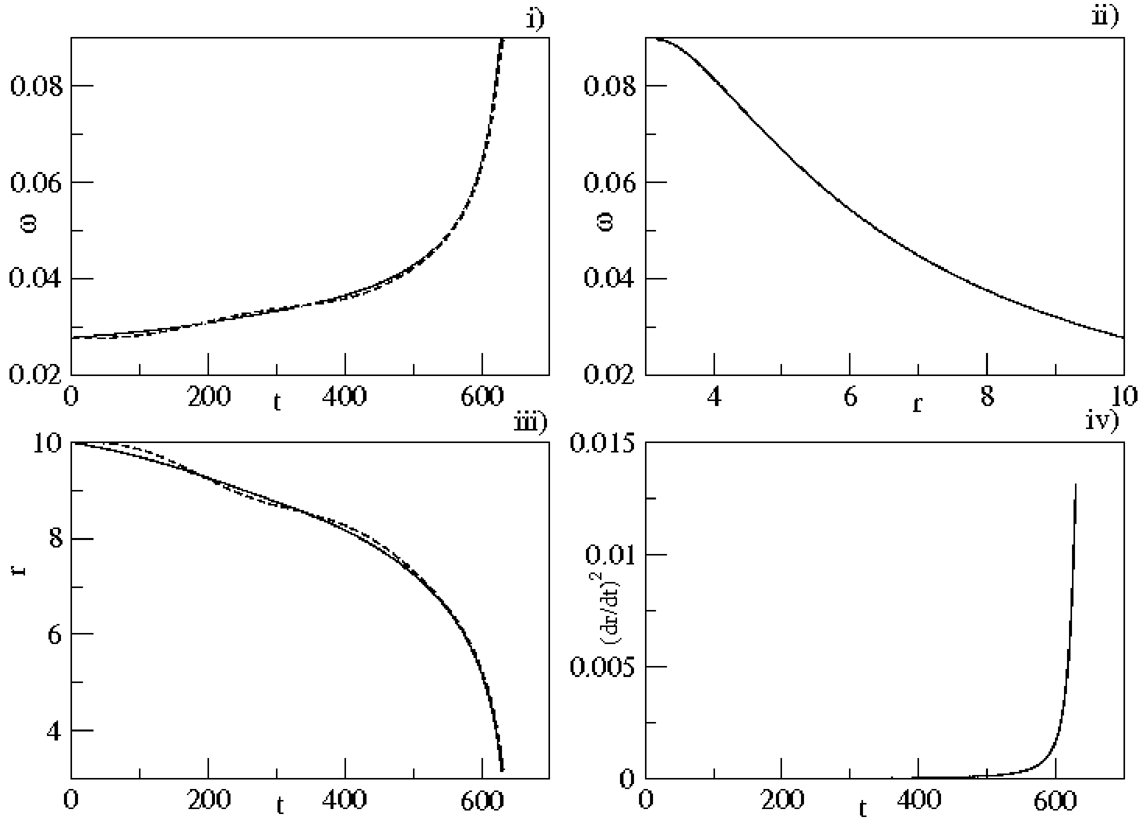

FIG. 2: Plots providing $\omega(t), \omega(r(t)), r(t)$ and $\dot{r}(t)^2$ for BBH evolution under SAPE [the binary configuration is same as in Fig. 1 and all quantities are dimensionless]. The rapid changes in ω, r and $\dot{r}^2$ occurring during the dynamical plunge is clearly visible and we terminate the SAPE when ω reaches its maximum value $\omega_{\rm mx}$. Though $\dot{r}^2 = (dr/dt)^2$ remains small near $\omega_{\rm mx}$, its magnitude changes roughly fivefold during the plunge under SAPE. The black-hole binary evolution that employs Eq. (31) for the initial value of p_r is displayed with thick line, while BBH evolution having $p_r = 0$ at the initial instant is displayed with dashed lines. The spurious eccentricity in SAPE is suppressed by using at $t = 0$ the expression for p_r, given by Eq. (31), and this is also reported in Ref. [19].

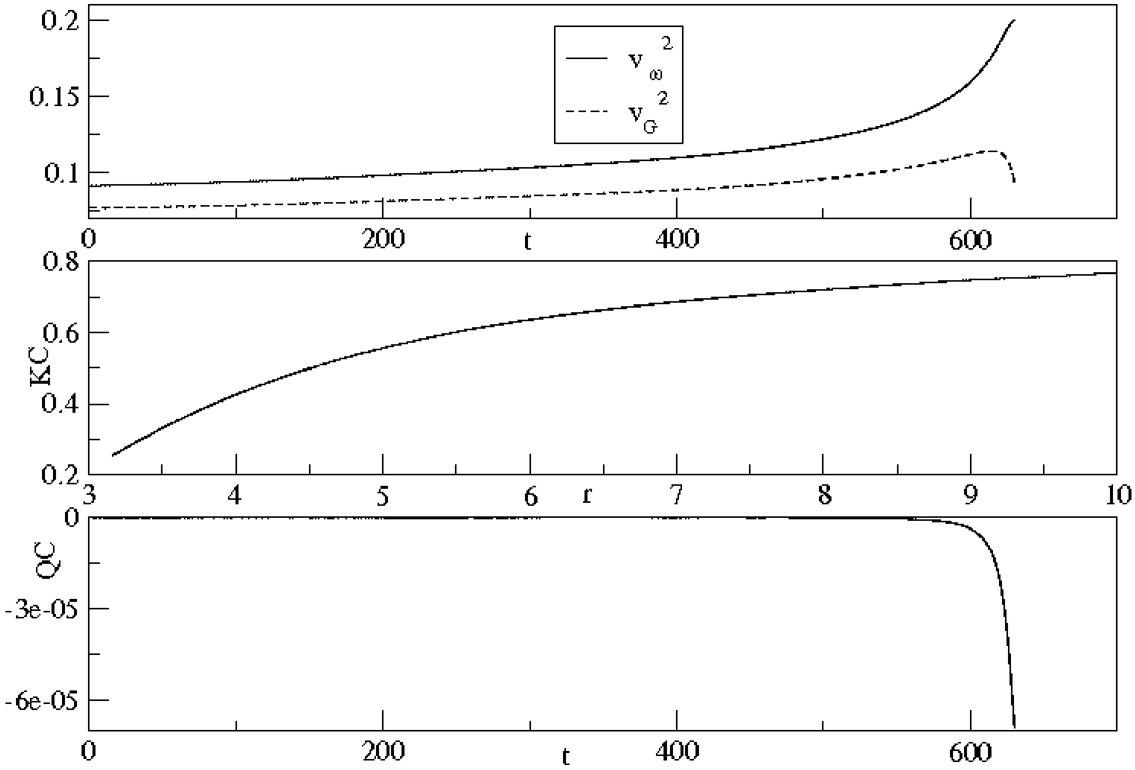

FIG. 3: Plots displaying reactive evolutions of few interesting dynamical quantities and relations in the SAPE [the binary configuration is same as in Fig. 1 and all quantities are dimensionless]. The top panel plots $v_\omega^2 = \omega^{2/3}, v_{\rm G}^2 = \dot{r}^2 + r^2\,\omega^2$. The strong r dependence of $v_{\rm G}^2$ makes it less attractive to characterize the orbital velocity compared to v_ω. In the middle panel, we plot the 'Kepler combination'(KC) $\omega^2\,r^3$ against r and a gradual decrease is clearly visible throughout the inspiral. The quasi-circularity (QC) condition $(d\,E - \bar{\omega}\,d\,j)$ is displayed in the bottom panel and its smallness justify the use of v_ω in the 3.5 PN accurate expression for dj/dt.

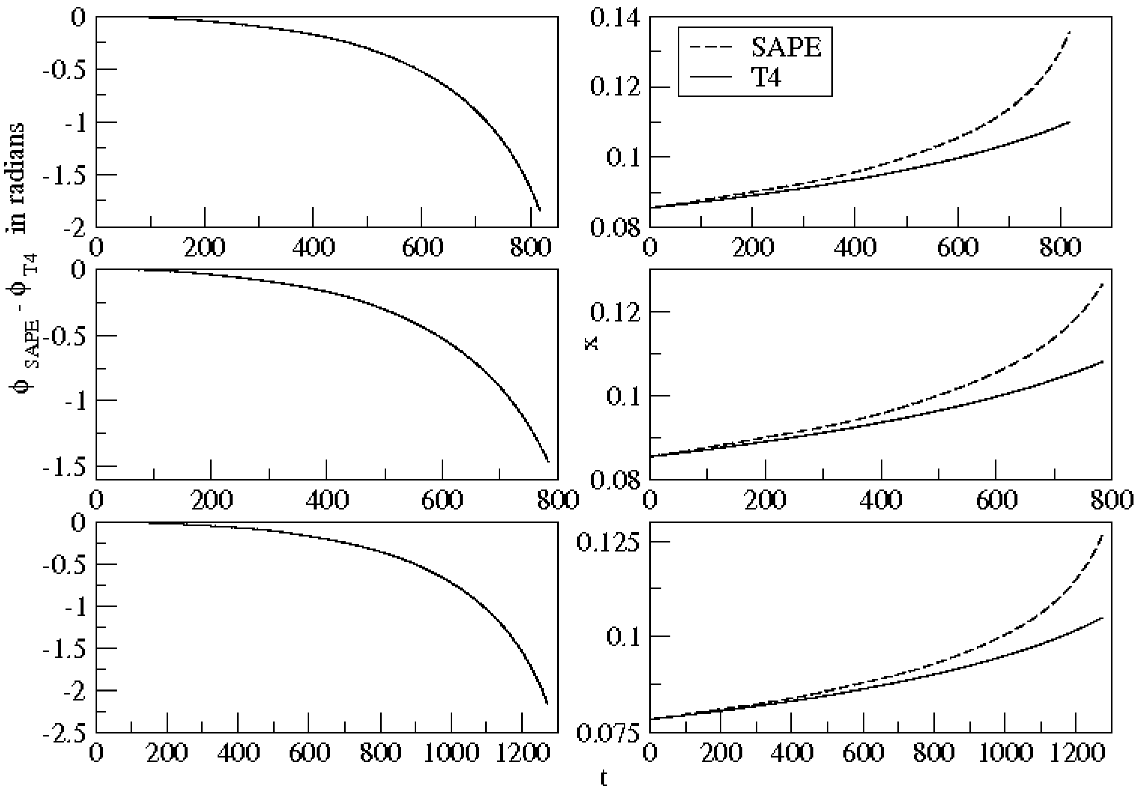

FIG. 4: Differences in the orbital phase evolutions associated with the SAPE and TaylorT4 approximant at 3.5PN order along with the associated $x \equiv \omega^{2/3}$ evolutions [recall that we have dropped *hat symbol* appearing in the dimensionless variables defined by Eq. (21)]. From the top to bottom panels. the orbital frequency ranges are $[0.025-0.05], [0.025-0.045]$ and $[0.022-0.045]$ respectively. The fractional differences in ϕ are $\sim 7\%, 5.8\%$ and $\sim 6.1\%$ in the above three cases. A sharp increase in $\phi_{\rm Sk}(t) - \phi_{\rm T4}(t)$ as we approach the plunge is also observed.

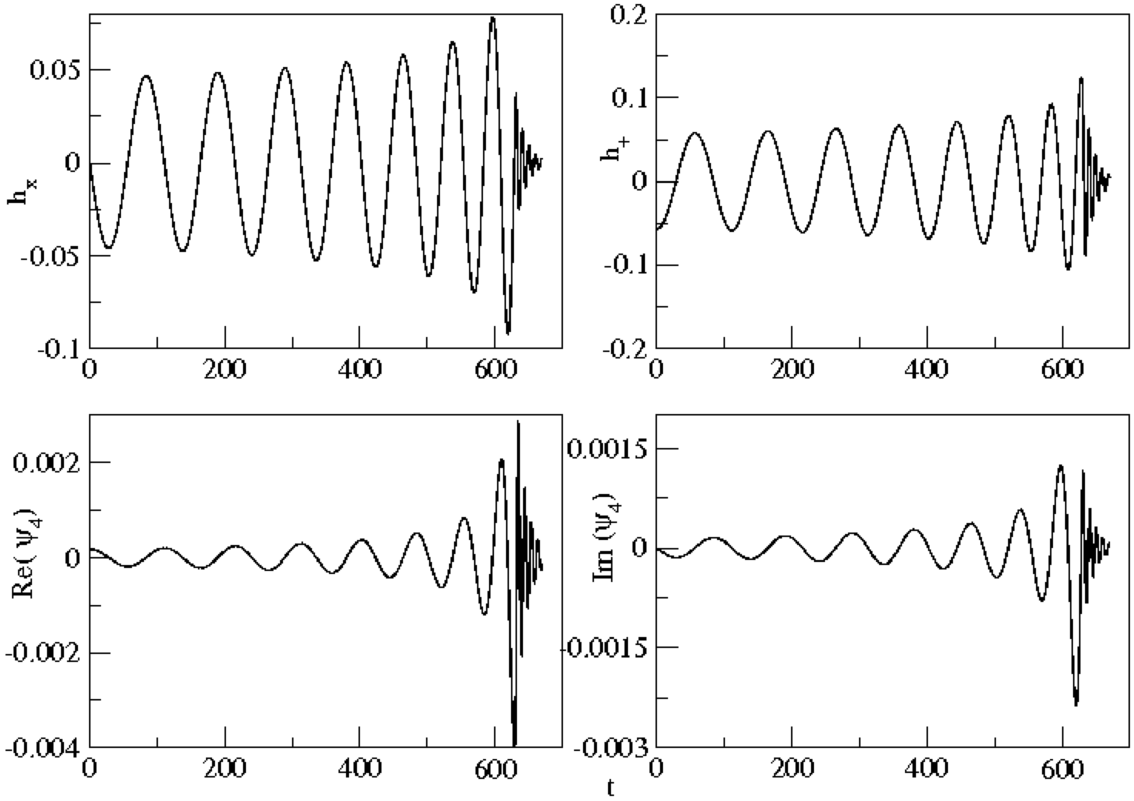

FIG. 5: Plots showing temporal evolution of scaled $h_{\times,+}$, $\Re(\psi_4)$ and $\Im(\psi_4)$ for equal mass binary black-hole coalescence in SAPE. We scale out $Gm/c^2\,r'$ from Eqs. (37) and (42) and let $i = \pi/3$. The matching to the QNMs is based on Ref. [7] (see Section IV and recall that t is identical to $\hat{t}$, defined by Eq. (21)).